Contents lists available at ScienceDirect

Chemical Engineering Research and Design

journal homepage: www.elsevier.com/locate/cherd

Modeling the solidification of O/W-emulsion droplet in solvent evaporation technique

Ting Shao[a,b], Lin Bai[a], Binhang Yan[a], Yong Jin[a], Yi Cheng[a,*]

[a] Department of Chemical Engineering, Tsinghua University, Beijing 100084, China
[b] Research Center of Laser Fusion, CAEP, P.O. Box 919-987, Mianyang 621900, China

ARTICLE INFO

Article history:
Received 29 September 2016
Received in revised form 7 April 2017
Accepted 19 April 2017
Available online 28 April 2017

Keywords:
Millimeter-sized polymer sphere
Solidification
Solvent evaporation
Mass transfer
Simulation

ABSTRACT

The removal of organic solvent plays an important role in the fabrication of polymer spheres by emulsion-based solvent evaporation technique. Mathematical model describing the mass transfer of fluorobenzene (FB) inside the O/W emulsion droplet, from the droplet to the continuous phase and from the continuous phase to the atmosphere to produce millimeter-sized polystyrene (PS) spheres was established. A novel approach based on finite volume method was developed to numerically solve the mathematical equations concerning the shrinkage of the solidifying droplet. Using this method, the variations of the droplet size and the concentration field inside the droplet were captured. The details of the solidification process which cannot be obtained using experimental methods were revealed. Several factors influencing the curing rate and mass transfer process, such as droplet number, initial droplet diameter, initial concentration and addition of FB in the continuous phase, were investigated in detail. The simulation results indicated that changing the initial concentration or changing the initial diameter of the droplet to tune the solidified particle size were essentially the same considering their effects on the details of the solidification process. When adding FB in the continuous phase to reduce the curing rate and concentration gradient, dispersing the added FB into droplets with the same diameter to that of the PS/FB droplet to be solidified has the most significant effect.

1. Introduction

Emulsion-based microencapsulation technique has wide applications in many areas such as drug delivery, pharmaceuticals, catalyst loading, biological engineering and food industry (Gharsallaoui et al., 2007; Lai and Tsiang, 2004; Nazzaro et al., 2012; Vasiliauskas et al., 2015; Wang, 2012). It is usually used to fabricate polymeric microspheres which encapsulate active or functional compounds in their matrix. Besides nano- and micron-scale particles frequently appeared in the literatures, polymer spheres with diameters in millimeters have their special applications in the area of high energy density physics, where they are used as cryogenic capsules for laser fusion experiments (Chen et al., 1991; Lambert et al., 1997; Paguio et al., 2006) or mandrels for the fabrication of inertial confinement fusion (ICF) targets which are capsules with nuclear fusion fuel encapsulated inside (Letts et al., 1995; McQuillan et al., 1997).

The fabrication of polymer spheres using microencapsulation technique usually consists of three steps: the emulsification of the polymer solution encapsulating other substance(s), the solidification of the polymer matrix, followed by the washing and drying of the solidified polymer spheres. Among these three steps, the second one is essentially important to determine the final morphology and microstructure of the polymer spheres, which will in turn influence the performance of the products in practical use (e.g., the encapsulation efficiency and the

Abbreviations: CP, continuous phase; DP, dispersed phase; FB, fluorobenzene; FVM, finite volume method; ICF, inertial confinement fusion; PαMS, poly(α-methylstyrene); PIV, particle image velocimetry; PLGA, poly(lactide-co-glycolide); PS, polystyrene; PVA, polyvinyl alcohol.

* *Corresponding author*. Fax: +86 10 6277 2051.
E-mail address: yicheng@tsinghua.edu.cn (Y. Cheng).

http://dx.doi.org/10.1016/j.cherd.2017.04.022

releasing profiles of the encapsulated drugs (Bile et al., 2015; Kiss et al., 2013; Mao et al., 2008; Vay et al., 2012; Yang et al., 2001). There are several ways to solidify the polymer matrix, such as in-situ polymerization, thermal-induced phase separation and solvent extraction/evaporation, among which the last one is the most straightforward and commonly used, especially in the fields of pharmaceutical industry and ICF targets fabrication (Bile et al., 2015; Freitas et al., 2005; Jyothi et al., 2010; Li et al., 2008; Michra et al., 2002; Vermillion et al., 2004). In the solvent evaporation method, the polymer is first dissolved in an organic solvent, forming a polymer solution which is subsequently dispersed as droplets (encapsulate other droplets with smaller sizes inside in some cases) in a water phase. The organic solvent is then removed from the dispersed oil phase to the continuous water phase and evaporates to the atmosphere thereafter, giving solidified polymer spheres. The mass transfer of the organic solvent in this process is key in determining the morphologies, structures and sometimes sizes of the solidified particles. For example, Izumikawa et al. (1991) has proved in their experiments that slow solidification at atmosphere pressure would produce particles with crystalline polymer matrices and rough surfaces while fast solidification at reduced pressure would produce amorphous particles with polymer matrices and smooth surfaces. Jeyanthi et al. (1996) adjusted the solvent removal rate by changing the bath temperature, and found that a rapid ramp of temperature resulted in spheres with large core and thin wall while a gradual temperature rise resulted in spheres with smaller core. For the fabrication of poly(α-methylstyrene) (PαMS) and PS spheres used for ICF targets, theoretical and experimental studies have revealed that the radial change of concentration determined the degree of the bumpiness around the surface of the spheres. Lowering the curing rate would benefit the improvement of the sphericity of the polymer spheres, which was a key index characterizing the performance of the product spheres (Subramanian et al., 2005).

The solidification of droplets using solvent evaporation technique is a typical mass transfer-controlled process. Up to now, researches about this process are mostly focused on the control of the overall curing rate and its influence on the morphologies or structures of the product spheres at macro-scale, while little attention has been paid to the kinetics inside each individual droplet at micro-scale. However, an improved understanding of the details of the mass transfer phenomenon at micro-scale and the kinetics of this process is in fact very important in many practical applications. For instance, the sphericity of the product solidified sphere used for ICF targets has a close relationship with the concentration field inside the solidifying droplet, just as mentioned above. Due to the technical difficulties of experimental investigations at the scale of single drop, the rarely existed researches on this aspect are mainly theoretical ones (Li et al., 1995a,b, 2008; Katou et al., 2008). A concrete model concerning the solidification of microspheres was built only by Li et al. (1995a,b) to our knowledge. A coordinate transformation was applied in their studies to deal with the moving boundary problem brought about by the shrinkage of the droplet during its solidification. Katou et al. (2008) developed a mathematical diffusion model to investigate the kinetics of solvent extraction/evaporation process for poly(lactide-*co*-glycolide) (PLGA) microparticle fabrication. However, the shrinkage of the droplet was not concerned in their work.

In the present work, we established a mathematical model to investigate the kinetics of solvent evaporation process with consideration of the diffusion inside the droplet, the mass transfer from the droplet to the surrounding phase and from the surrounding phase to the atmosphere. Instead of applying complex coordinate transformation, a novel strategy numerically solving the mathematical model was proposed concerning the shrinkage of the solidifying droplet. The fabrication of millimeter-sized PS spheres used for ICF targets was employed as the research object. Using the mathematical model and the corresponding solving strategy, the kinetics of the solidification process and the factors influencing them were investigated in detail.

2. Mathematical model

2.1. Governing equation of mass transfer

Fig. 1 illustrates schematically the solidification process of O/W emulsion droplet using solvent evaporation method which happened in a rotating flask. The organic solvent, i.e., FB in this work, is first extracted from the droplet (DP) into the continuous phase (CP) and then evaporates from the CP into the atmosphere. As the solvent diffuses out, the droplet size becomes smaller while the PS (Mw 250,000) concentration gets higher until it solidifies. Since the fluid flow in the continuous phase is quite moderate, and the viscosity ratio of DP to CP is high, we can infer that there would be no bulk flow inside the droplet (Bryden and Brenner, 1999; Shao et al., 2012). Therefore, the mass transfer model of FB in the droplet phase can be established with the following reasonable assumptions: first, the droplet is an ideal sphere; second, there is no bulk flow in the DP where the mass transfer is accomplished by molecular diffusion; third, the system is in quasi steady state; fourth, the concentration of FB at the two sides of the liquid–liquid interface was in balance with each other; and last, the thickness of the film for interphase mass transfer, δ_m, is thin enough to be ignored, which is to say that the organic solvent is distributed uniformly in the CP.

$$\frac{\partial C_d(r,t)}{\partial t} = \frac{1}{r^2}\frac{\partial}{\partial r}\left(r^2 D_A \frac{\partial C_d(r,t)}{\partial r}\right), 0 < r < R(t),\ t > 0 \quad (1)$$

where $C_d(r, t)$ is the molar volume concentration of FB at radius r and time t inside the droplet; the center of the droplet is considered as the original point; R is the radius of the droplet at time t, which will constantly change with the solvent diffusing out; D_A represents the diffusion coefficient of FB in the DP, which is a function of $C_d(r, t)$. All the parameters mentioned above are illustrated in Fig. 1(b).

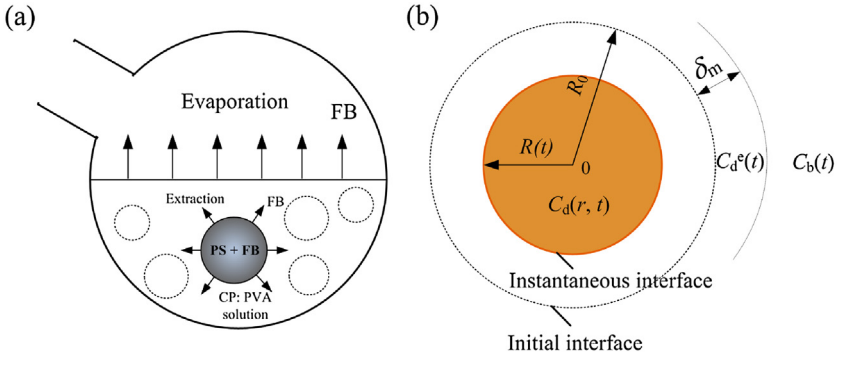

Fig. 1 – Schematic of the solidification process of O/W emulsion droplet using solvent evaporation method.

The initial condition of the above equation is:

$$C_d(r, 0) = C_{d0}, 0 \le r \le R(t) \quad (1a)$$

And the boundary conditions are:

$$\frac{\partial C_d}{\partial r}|r = 0 = 0 \quad (1b)$$

$$-D_A \frac{\partial C_d}{\partial r}|r = R = k_c (HC_d(R, t) - C_b(t)) \quad (1c)$$

where k_c is the interphase mass transfer coefficient of FB between DP and CP. H is the phase equilibrium coefficient of FB at the two sides of the liquid–liquid interface. C_b is the bulk concentration of FB in the CP.

Another equation is the mass conservation equation of FB in the continuous phase:

$$V_T \frac{dC_b}{dt} = N \cdot 4\pi R^2 \cdot k_c (HC_d(R, t) - C_b(t)) - K_y \quad (2)$$

where V_T is the total volume of the CP; N denotes the number of the droplets to be solidified; K_y is the evaporating rate of FB from the CP to the atmosphere.

For the CP which is not pre-saturated with FB, the initial condition of Eq. (2) is as follows:

$$C_b(0) = 0 \quad (2a)$$

2.2. Determination of model parameters

2.2.1. Convective mass transfer coefficient, k_c

k_c was formulated using an empirical equation for spherical particles suspended in an agitated vessel (Li et al., 1995a):

$$k_c' = \frac{\rho_c D_{AC}}{R}(2+0.6Re_c^{0.5}Sc^{0.33}) \quad (3)$$

ρ_c is the density of the CP. In the present study, a 0.5% w/v aqueous solution of polyvinyl alcohol (PVA, Mw 75,000, 88% hydrolyzed) was used as CP. The density of this solution was measured as 989.1 kg/m^3 by digital density meter (DDM 2910, Rudolf Chemie). D_{AC} is the diffusion coefficient of component A (FB in our research) in the CP, i.e., 0.676×10^{-9} m^2/s according to Hayduk–Laudle equation. $Sc = \mu_c/(\rho_c D_{AC}) = 1.79 \times 10^3$. The Reynolds number $Re_c = 2Ru_c\rho_c/\mu_c$, where u_c is the fluid velocity of the CP. In this study, u_c was estimated to be 0.04 m/s based on the PIV (Particle Image Velocimetry) results.

Formula (3) gives the mass transfer coefficient, k_c', with the unit of kg/m^2/s. Since the solubility of FB in the water phase is very low, k_c' can be transferred into k_c with the unit of m/s as follows:

$$k_c = k_c' \frac{M_s}{\rho_c \times 10^3[\text{kg/m}^3]/[\text{g/cm}^3]} \quad (4)$$

where M_s is the molecular weight of FB.

2.2.2. Evaporation rate of FB from CP to atmosphere, K_y

K_y was experimentally measured with the method similar to Li et al. (1995a). 80 mL of 0.5% w/v PVA was quantitatively transferred to two flasks. Then, a desired amount of FB was added to one flask and dispersed into fine droplets in the water phase as uniformly as possible. The other sample with no FB added served as a control. The two flasks were placed in an open environment with exactly the same conditions of 50 °C and 100 rpm magnetic stirring rate. Both flasks were weighed every 20 or 10 min to determine the total evaporated amount of FB, as shown in Fig. 2.

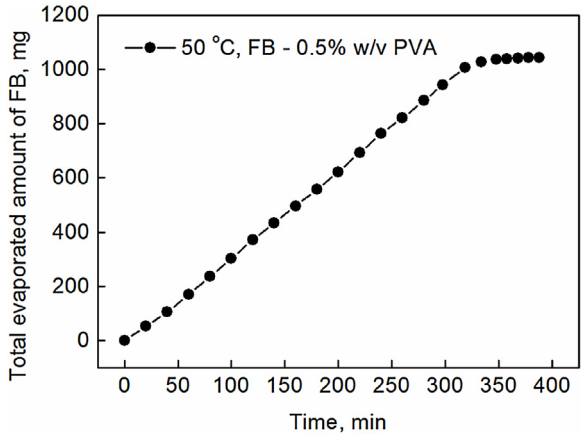

Fig. 2 – Evaporation of FB in 40 mL 0.5% w/v PVA solution at 50 °C.

It is evident from Fig. 2 that there are two stages of evaporation. For the first one, the amount of the evaporated FB increases linearly with respect of time. The 0.5% w/v PVA solution was saturated with FB at this stage, for many FB droplets were observed suspending in the water phase. Since the concentration of FB dissolved in the water phase is constant throughout this stage, the evaporation rate is a constant as well:

$$K_y = K_y' C_b^s = \text{constant} \quad (5)$$

where C_b^s is the saturated concentration of FB in the 0.5% w/v PVA solution. The values of K_y and K_y' can be obtained as 5.6×10^{-7} mol s^{-1} and 2.9×10^{-8} m^3 s^{-1} respectively by linear fitting of the experimental data.

At the second stage, no FB droplets were observed while the solution became clear, which implied that the water phase was under-saturated with FB. The FB concentration should satisfy the following equation:

$$V_T \frac{dC_b}{dt} = -K_y' C_b \quad (6)$$

K_y' in Eq. (6) was found to be 2.9×10^{-8} m^3 s^{-1} by curve fitting, which was the same as that obtained for the first stage. Therefore, the evaporation rate of FB in 0.5% w/v PVA solution can be expressed as:

$$K_y = K_y' C_b = 2.9 \times 10^{-8}\ \text{m}^3\ \text{s}^{-1} \cdot C_b \quad (7)$$

2.2.3. Diffusion coefficient of FB in the droplet phase, D_A

The droplet phase mainly consists of two components: organic solvent FB and polymer PS. The diffusion coefficient of solvent–polymer system is highly concentration dependent (Li et al., 1995a). The relationship between D_A and the polymer concentration was suggested by Reuvers and Smolders (1987) as follows:

$$D_A = r_1 10^{-(r_2 + r_3\phi_P)} \quad (8)$$

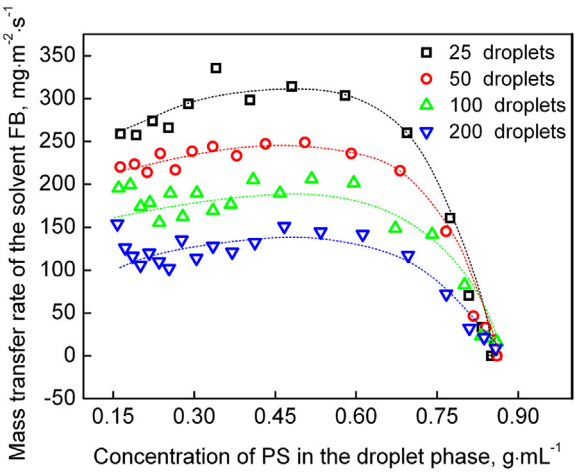

Fig. 3 – Apparent mass transfer rate of FB from the droplet to CP calculated from experimental results.

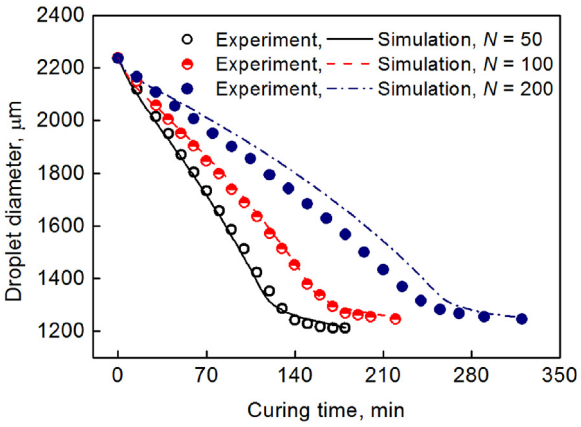

Fig. 4 – Comparison of droplet diameters versus curing time for N = 50, N = 100 and N = 200 respectively, where N denotes the number of the solidifying droplets.

where ϕ_p is the volume fraction of the polymer. Since the parameters r_1, r_2 and r_3 are constants depending on the system, Eq. (8) could be rewritten in the form of:

$$D_A = a10^{-b\phi_P} \tag{9}$$

where a equal to $r_1 10^{-r_2}$ and b equal to r_3 are constants. In our research, the densities of PS, FB and PS-FB solution are quite close to each other. Therefore, ϕ_p can be expressed as a function of C_d as:

$$\phi_p = 1 - \frac{M_s \times 10^{-3}\,[\mathrm{kg/mol}] \cdot C_d}{\rho_s \times 10^3\,\left[\mathrm{kg/m^3}\right] / \left[\mathrm{g/cm^3}\right]} \tag{10}$$

2.2.4. *Phase equilibrium coefficient of FB, H*

H describes the relationship between $C_d(R, t)$ and $C_d^e(t)$ (as shown in Fig. 1(b)). Fig. 3 gives the apparent average mass transfer rate of FB from CP to DP calculated from the experimentally measured droplet sizes versus curing time. It can be observed clearly from this figure that no matter how many droplets were cured simultaneously in a batch, the apparent average mass transfer rates did not change remarkably at the initial and middle stages. Instead, they all decreased significantly when the average concentration of PS in the droplet phase increased approximately to 0.75 g mL^{-1}. It can be assumed reasonably from this phenomenon that the concentration of FB at the CP side of the film, $C_d^e(t)$, remained unchanged (i.e., this side was FB-saturated) until that at the droplet side, $C_d(R, t)$, decreased to a critical value C_s (approximately 1804 mol m^{-3} calculated from the PS concentration 0.75 g mL^{-1}). Another assumption is that when $C_d(R, t)$ was lower than C_s, $C_d^e(t)$ had a linear relationship with $C_d(R, t)$. So, the phase equilibrium coefficient, H, can be expressed mathematically as follows:

$$\begin{aligned} &C_d^e(t) = C_b^s; C_d(R, t) \geq C_s \\ &H = C_b^s \cdot M_s \times 10^{-3}/\rho_s; C_d(R, t) < C_s \end{aligned} \tag{11}$$

where C_b^s is the saturated concentration of FB in the CP; ρ_s is the density of FB at 50 °C with the unit of kg m^{-3}.

The finite volume method (FVM) was adopted to numerically solve the mathematical model established above. The droplet was divided into 100 discrete shell layers along its radius with equal length step at first. Different from most problems solved by FVM in the literature, the length step in the present case was not fixed throughout the solidification process. Instead, it would vary with time since the droplet gets smaller with the solvent diffusing out. Consequently, the size and concentration field cannot be obtained directly. To get over this obstacle, the so-called fictitious concentration was introduced to capture the variation of the size of each shell layer and thus the shrinkage of the droplet. For each shell layer, the flux of FB during a time step was first obtained by solving the discrete equations. Given the concentration and volume of the shell layer at the current time step as well as the relationship between the density and concentration of the solution, the concentration and volume at the next time step can be obtained. The details of the numerical method and solving strategy are given in Appendix A.

3. Results and discussion

3.1. *Validation of the model and solving strategy*

The numerical simulations are validated by the experimental results in terms of the profiles of the droplet diameters. The comparison of the profiles of droplet diameters versus curing time at three different experimental conditions is shown in Fig. 4. As can be clearly seen in this figure, the numerical simulation results have reasonably good agreement with those of the experiments, though some errors can be justified.

3.2. *Factors that influence the solidification process*

Although the apparent mass transfer rate can be estimated from the experimental results, the details which may influence the ultimate morphologies of the solidified particles cannot be obtained. Using the numerical simulation method proposed above, several factors influencing the mass transfer of FB will be investigated in detail in this section.

3.2.1. *Number of the droplets to be solidified*

It is already known from Fig. 4 that the apparent mass transfer rate would decrease with increased number of the droplets. Fig. 5 gives the radial distribution of residual FB inside the droplets at different curing times. It is clear that the four images in this figure show a similar appearance. The residual FB distributes nearly uniformly and the gradients increase slowly at the initial stage when the droplet radius is no larger

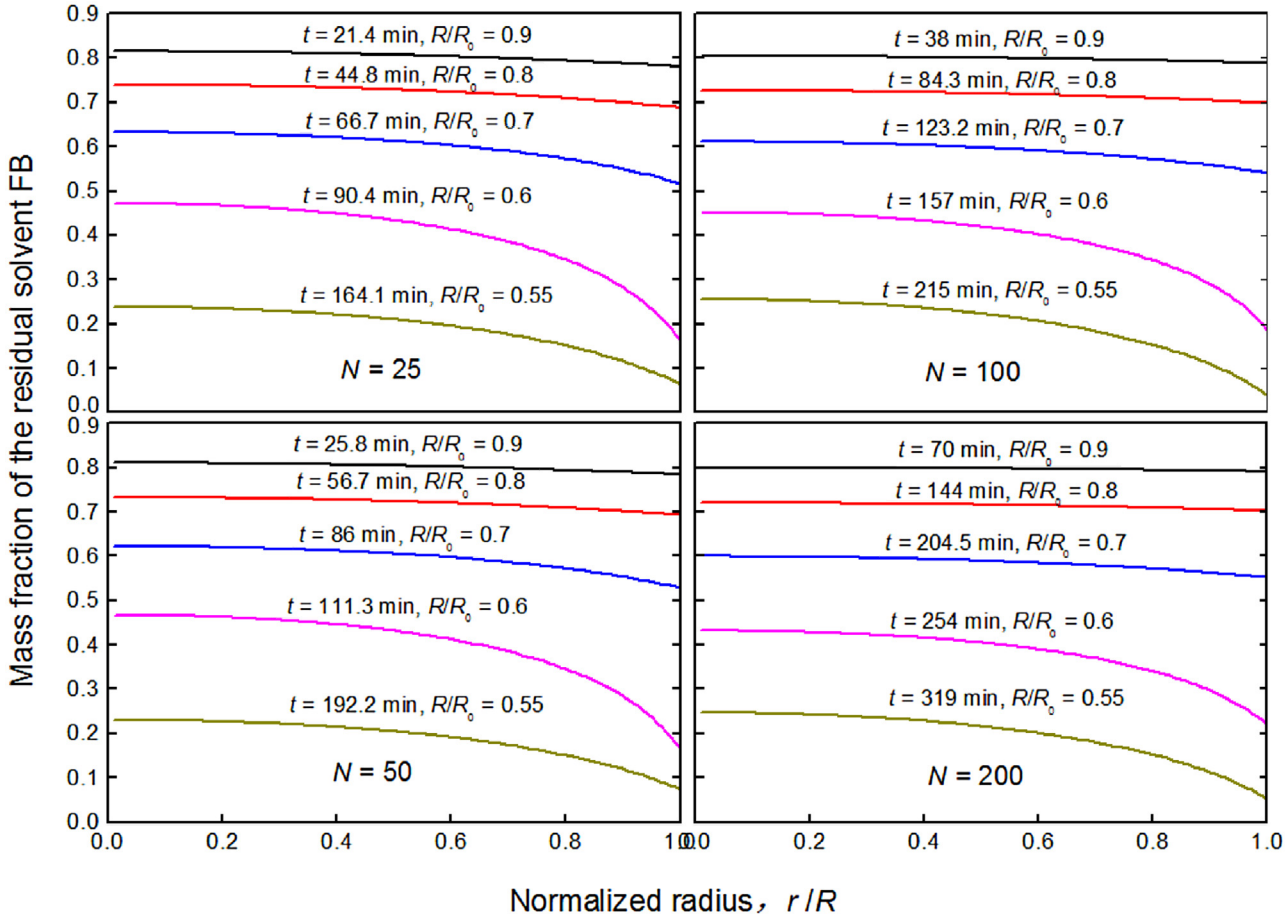

Fig. 5 – Radial distribution of the residual organic solvent in the droplet at different curing time.

than $0.7R_0$. However, the concentration gradient increases significantly faster as the droplet gets smaller. When the droplet diameter decreases to 0.6 times of its initial value, the mass fraction difference between the center and boundary of the droplet is even higher than 20 wt%. On the other hand, for each individual curve, the concentration gradient at the boundary area is higher than that at the central area. It can be identified by comparing the four images qualitatively that the concentration gradient of the residual FB would decrease to a certain extent as the droplet number increases.

To compare the concentration gradients more straightforwardly, the mass fraction-based average gradient is defined as follows:

$$d\overline{w} = \frac{w_d(0) - w_d(R)}{R} \tag{12}$$

where w_d is the mass fraction of the residual solvent. Based on this definition, the variation of the average concentration gradient versus the normalized droplet diameter at the four different conditions mentioned above is shown in Fig. 6. It can be seen from this figure that the concentration gradient of the residual solvent first increases and then decreases as the solidification proceeds. Comparison of the four curves indicates that increasing the solidified droplets number will decrease the average gradient obviously.

The significant effect of the droplets number on the mass transfer rate can be explained by the concentration of FB dissolved in the CP. As Fig. 7 shows, the concentration of FB in CP increases significantly with increasing droplets number, which will definitely lead to reduction of the concentration

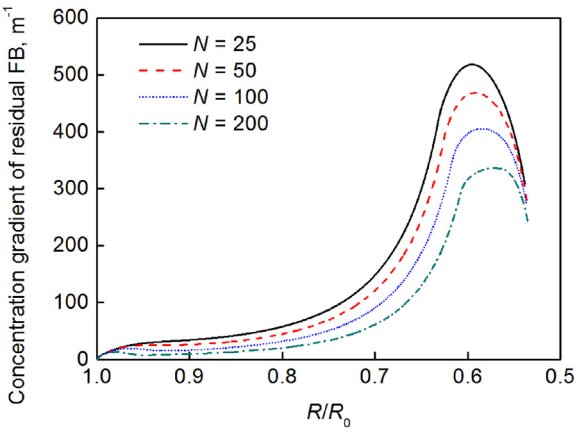

Fig. 6 – Average concentration gradient of the residual solvent defined in Eq. (12) versus the normalized droplet diameter for N = 25, N = 50, N = 100 and N = 200 respectively.

difference between the film and bulk phase. With the mass transfer coefficient fixed, the reduction of concentration difference will decrease the mass transfer rate directly.

3.2.2. *Addition of FB in the continuous phase*

Besides tuning the number of the droplets to be solidified, another similar way to adjust the curing rate is to directly add pure FB droplets in CP. It is undoubted that the more FB is added, the more significantly the mass transfer rate will decrease. So, the effect of the added FB quantity is not investigated here. Instead, influences of the initial diameters of the added FB droplets are compared with the basis that the total

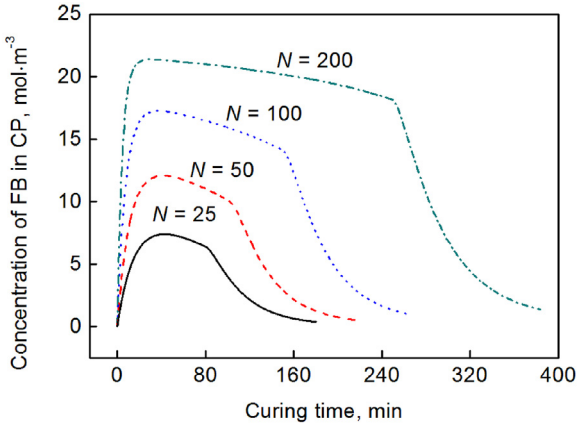

Fig. 7 – Concentration of the organic solvent dissolved in CP versus curing time for $N = 25$, $N = 50$, $N = 100$ and $N = 200$ respectively.

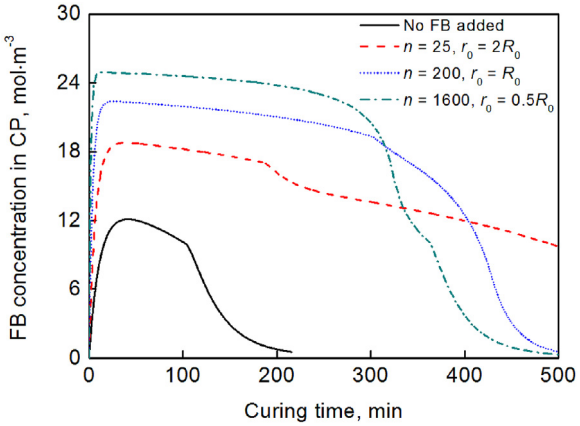

Fig. 9 – Concentration of the organic solvent dissolved in CP versus curing time for no FB added; $n = 25$, $r_0 = 2R_0$; $n = 200$, $r_0 = R_0$ and $n = 1600$, $r_0 = 0.5R_0$ respectively.

mass of these FB droplets is fixed. In the following, the number and initial diameter of the added FB droplets are denoted as n and r_0 respectively, while the initial diameter of the PS/FB droplets is denoted as R_0. Three different ways are adopted to add a certain amount of FB in CP where $n = 25$, $r_0 = 2R_0$ (Case 1); $n = 200$, $r_0 = R_0$ (Case 2); and $n = 1600$, $r_0 = 0.5R_0$ (Case 3) respectively.

The influence of the addition of FB in CP on the local curing rate, ζ (mol m^{-3} s^{-1}), is firstly investigated where ζ is defined as follows:

$$\zeta = -\frac{dC_d}{dt} \tag{13}$$

As seen in Fig. 8, adding FB in these three ways will all lower the curing rate compared with the condition where no FB is added. Nevertheless, there still exists remarkable difference among these ways. When the FB droplets have an initial diameter of $0.5R_0$, its effect on the curing rate is significant at the initial stage but becomes weaker as the solidification proceeds. The curing rates at the middle and final stages are quite close and even equal to those of the condition where no FB is added. However, when the added droplets diameters are equal to or larger than R_0, their influence on the curing rate lasts throughout the whole curing process. These two cases show a similar tendency where the influence at the initial stage is much more significant than that at the final stage. Compared to Case 1, Case 2 has an even more significant effect, which is to say, from the decreasing-curing-rate point of view, the way where the added FB droplets have an initial diameter to that of the solidified PS/FB droplets has a best effect.

The results shown in Fig. 8 are consistent with the variations of FB concentration dissolved in CP illustrated in Fig. 9. As this figure shows, adding a certain amount of FB in CP can increase the dissolved FB concentration remarkably, no matter how the added FB is dispersed. On the other hand, when the dispersed FB droplets have a small diameter, the high mass transfer rate brought about by their high specific surface areas leads to a high increase of FB concentration in CP. However, since the FB droplets will be consumed shortly after their addition with such high mass transfer rate, the FB concentration in CP will decrease rapidly thereafter. As a result, the curing rates of the PS/FB droplets will increase until they are equal to those of the condition where no FB is added, just as the green lines show in Fig. 10. With the increase of the FB droplets diameters, the variation of FB concentration in CP throughout the whole solidification process becomes milder. However, increasing diameter suppresses the increasing amplitude of FB concentration in CP as well, as Fig. 11 illustrates. So, increasing added FB droplet diameter further (i.e., from $r_0 = R_0$ to $r_0 = 2R_0$) will weaken its effect on reducing the curing rate of PS/FB droplet instead.

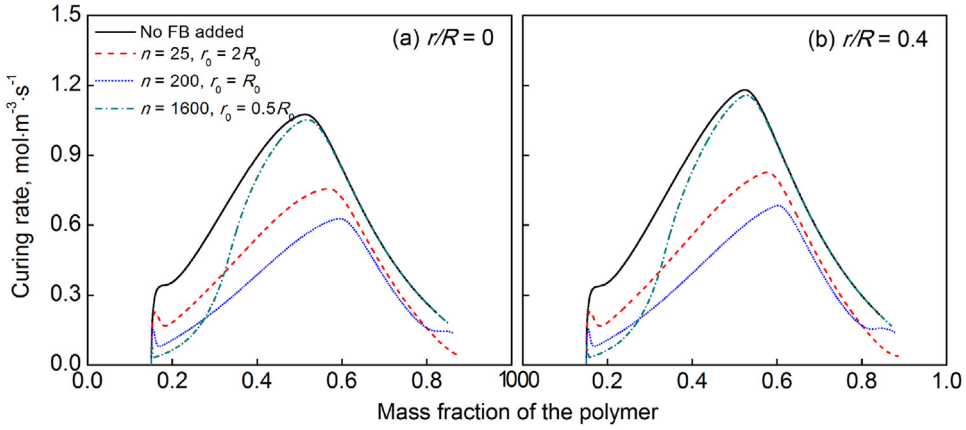

Fig. 8 – Comparison of the effect of adding FB in CP with different ways using curing rate defined in Eq. (13) in certain areas of the droplet. (a) The area where $r/R = 0$; (b) the area where $r/R = 0.4$. The number of the droplets to be solidified is $N = 50$, and the volume of the continuous phase is 40 mL in all cases.

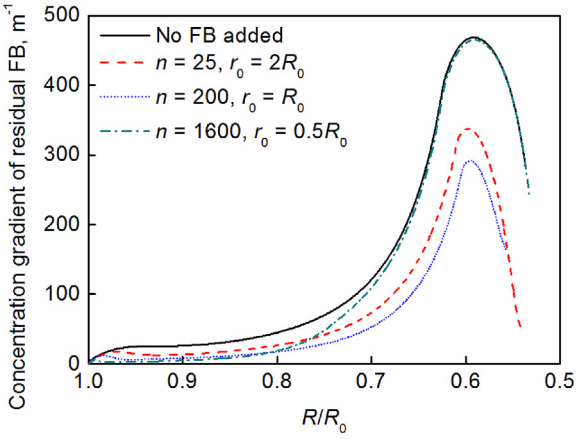

Fig. 10 – Average concentration gradient of the residual solvent defined in Eq. (12) versus the normalized droplet diameter for no FB added; $n = 25$, $r_0 = 2R_0$; $n = 200$, $r_0 = R_0$ and $n = 1600$, $r_0 = 0.5R_0$ respectively. (For interpretation of the references to color in the text, the reader is referred to the web version of this article.)

Fig. 10 gives the average concentration gradients of the residual solvent along the radial direction. Similar to the results shown in Fig. 6, the concentration gradients first increase and reach their individual peak values at about $R/R_0 = 0.6$ and then decrease. Compared to the condition where no FB is added, adding a certain amount of FB in CP in the three ways mentioned above all reduces the gradients. When the FB droplets have an initial diameter of $0.5R_0$, they have obvious influence on the gradient only before R/R_0 decreases approximately to 0.7, while the influence after that is almost undetectable. Among the three ways, Case 2 has the most significant effect on the concentration gradients.

3.2.3. *Diameter of the solidified particle, d_p*

There are two ways to tune the final diameter of the solidified particle in practice. One is to change the initial concentration of the polymer in the droplet. The other is to directly change the initial diameter of the droplet. In this section, the effects of these two methods on the mass transfer will be investigated respectively and the probable differences will be analyzed.

For the initial concentration-verified case, the initial diameter of the droplet is 2.24 mm, and the initial concentrations of PS are 5 wt%, 10 wt%, 15 wt% and 20 wt% respectively. As a comparison, the initial PS concentration for the initial diameter-verified case is 15 wt% and the initial diameters are 1.55 mm, 1.95 mm, 2.24 mm and 2.46 mm respectively to make sure that the final diameters of the solidified particles in this case are respectively the same to those of the four conditions in the above case. The effects of the initial concentration as well as the initial diameter of the droplets on the concentration gradient, curing rate and concentration of FB dissolved in CP are shown in Figs. 11–13 respectively. It can be clearly seen from Fig. 11 that increasing the initial mass fraction of FB and decreasing the initial diameter of the droplet will both increase the average concentration gradient of FB. Besides the same tendency revealed by Fig. 11(a) and (b), another interesting phenomenon is that the curves in these two subfigures nearly coincide with each other except for the different starting points brought about by the different initial concentrations in Fig. 11(a). Fig. 13 reveals the effect of the particle diameter on the FB concentration in CP. The general tendency is that increasing the final diameter of the solidified particle will increase the FB concentration in CP, mainly at the middle stage of the solidification process. The curves in Fig. 13(b) are quite close to those in Fig. 13(a) except for the parts before the average mass fraction of PS reaches 0.3. The divergence which appears before this point is caused by the difference of the initial concentration. With the same initial diameter, the higher the initial mass fraction of FB is, the more organic solvent should be removed before the average concentration reached a certain value, which causes higher concentration of FB in CP. Fig. 12 shows the influence of d_p on the curing rate in each local area. It is obvious that as d_p decreases, the curing rate will increase, no matter which method is adopted to tune d_p. Again, the curves in Fig. 12(b) are quite close to the ones in Fig. 12(a). The comparison of the subfigures (a) and (b) in these three figures respectively implies that the two ways adjusting the final diameter of the solidified particle actually have similar effects on the mass transfer of the solidification process. That is to say, once the final diameter of the solidified particle is fixed, the mass transfer as well as the distribution of FB during the solidification process is also fixed, no matter what the initial concentration and diameter of the droplet are. The two methods tuning the diameter of the solidified particle have no essential difference.

Another interesting phenomenon as Fig. 12 shows is that for a specified individual area of the droplet, the peak values of the curing rates appear at the same PS mass fraction though the initial concentration or diameter varies.

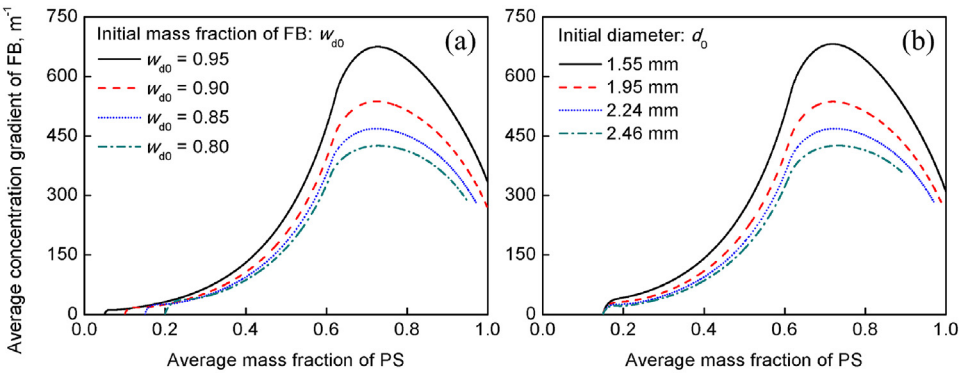

Fig. 11 – Effect of the final diameter of the solidified particle adjusted by (a) the initial concentration of polymer in DP, and (b) the initial diameter of the droplet to be solidified on the variation of the average concentration gradient of the residual solvent defined in Eq. (12) versus the average mass fraction of PS in the solidifying droplet.

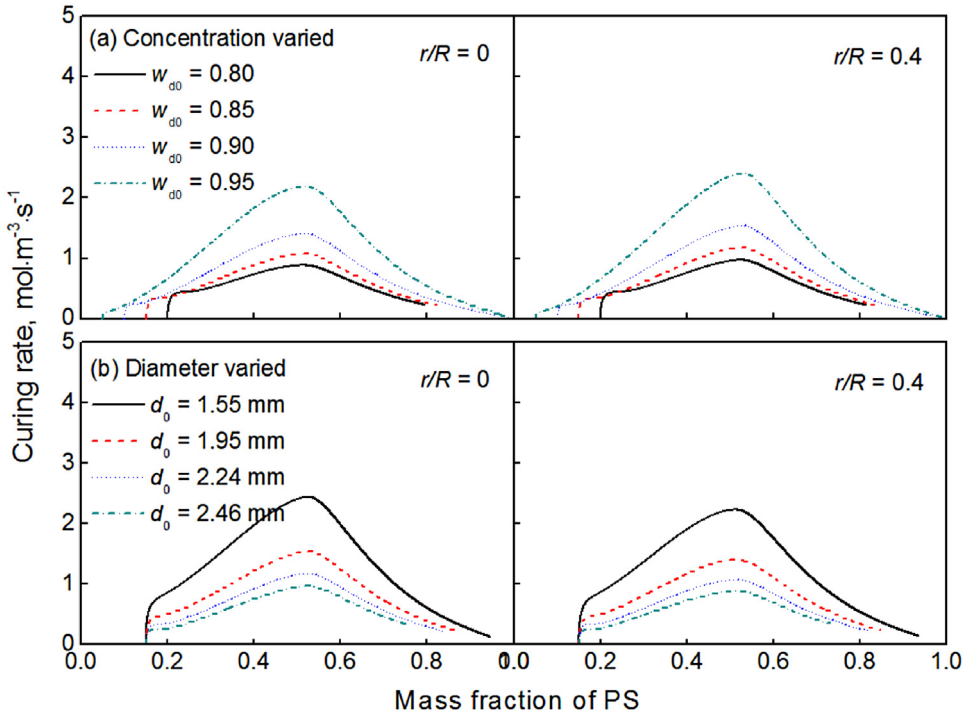

Fig. 12 – Effect of the final diameter of the solidified particle adjusted by (a) the initial concentration of polymer in DP, and (b) the initial diameter of the droplet to be solidified on the curing rate defined in Eq. (13) in different areas of the droplet.

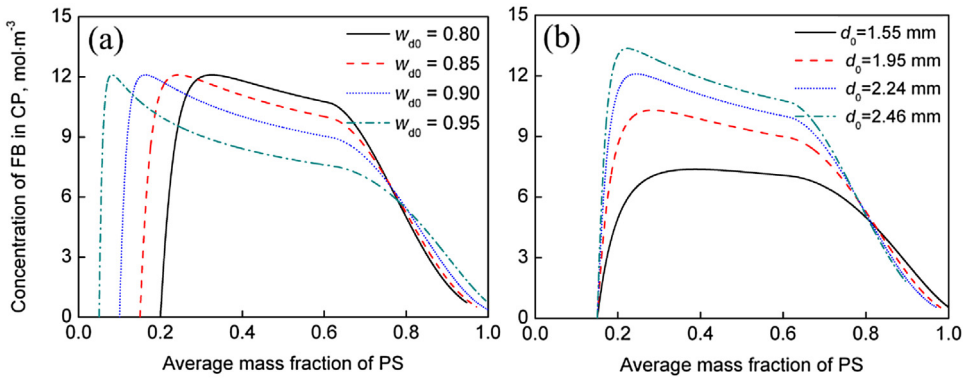

Fig. 13 – Effect of the final diameter of the solidified particle adjusted by (a) the initial concentration of polymer in DP, and (b) the initial diameter of the droplet to be solidified on the concentration of FB dissolved in CP.

4. Conclusions

A mathematical model describing the formation of polystyrene spheres by solvent extraction/evaporation method has been established based on the mass transfer of the organic solvent FB. Parameters in the model were determined or estimated according to the related literatures and experiments performed in the present work. A novel strategy numerically solving the mathematical model was proposed and implemented on the basis of the Finite Volume Method, where the variations of the sizes and concentration fields in the droplet were captured by introducing "fictitious concentration". The numerical results were in good agreement with the experimental ones in terms of the diameter variations of the solidifying droplets, which validated the model and solving strategy proposed here. Using this simulation method, several factors influencing the mass transfer process, including solidifying droplet numbers, addition of organic solvent in the continuous phase, initial diameters and initial concentrations, were investigated successfully in detail. The following conclusions can be drawn from the numerical simulations:

(1) The residual organic solvent FB in the droplet is not uniformly distributed. The concentration gradient of FB in the outer layer of the droplet is much higher than that in the central area. Correspondingly, curing rates in different areas also differ from each other.
(2) With the curing temperature and volume of the CP fixed, increasing the solidifying droplet numbers, increasing the initial concentration of polymer in the droplet, increasing the initial droplet diameter or adding organic solvent in CP can all decrease the concentration gradient as well as curing rate. Adjusting the initial concentration and the initial diameter of the droplet to change the final diameter of the solidified particle are essentially the same even considering their effects on the details of the mass transfer at micro-scale.
(3) Adding FB in CP in forms of dispersed droplets is an effective way to reduce the curing rate and concentration gradient. For a certain amount of FB, dispersing it into

droplets with the same diameters to those of the PS/FB droplets to be solidified has the most significant effect.

The presented approach can be useful for better control of PS sphere fabrication process. It is also applicable for the fabrication of millimeter-sized hollow PS spheres and other microparticle fabrication processes by solvent evaporation.

Acknowledgements

Financial supports from National 973 Project of PR China (No. 2013CB733604), National Natural Science Foundation (No. 21576151) and Science and Technology Development Foundation of China Academy of Engineering Physics (No. 2015B0302071) are acknowledged.

Appendix A.

The finite volume method was adopted to discrete Eq. (1). The droplet was divided into k segments (shell layers in practice) along its radius as shown in Fig. A1, forming k nodes and $k+1$ interfaces. Each node represented a control volume. For instance, in Fig. A1, node P which locates at the middle of segment "we" represents the control volume P enclosed by the interfaces w and e. W and E are its two adjacent nodes, or in other words, control volumes. Concentration was uniform throughout the control volume, denoted as C_{dP}.

For control volume P in Fig. A1, the discrete equation of Eq. (1) can be written in the form of:

$$a_1 C_{dW}^{*}(\mathrm{tr}) + a_2 C_{dP}^{*}(\mathrm{tr}) + a_3 C_{dE}^{*}(\mathrm{tr}) = b \tag{A1}$$

where a_1, a_2 and b are constants which are the functions of the time step Δt, length step ${r_e}^0$ and ${r_w}^0$, and diffusion coefficient ${D_{Aw}}^0$ and ${D_{Ae}}^0$. The superscripts "0" and "*" denote the current time t and the following time $t+\Delta t$ respectively.

Since the droplet would get smaller with FB diffusing out, the size of each control volume would change as well. Thus, the variation of the concentration of FB in the control volume actually stem from two factors: one is the decrease of the amount of the residual FB caused by diffusion, while the other is the variation of the volume of the control volume. Therefore, solving the discrete equations with the form of Eq. (A1) would not give the real value of ${C_{dP}}^{*}$ in the present case. Instead, it would give a so-called fictitious concentration denoted as ${C_{dP}}^{*}(\mathrm{tr})$ as shown in Eq. (A1). Nevertheless, the flux of FB during a time step Δt can be obtained with ${C_{dP}}^{*}(\mathrm{tr})$ known. The mass of FB as well as the total mass of the solution in the control volume will be obtained thereafter, which gives the mass fraction of FB. With the functional relationship between the density of the solution and the mass fraction of FB, variation of the volume of the control volume and thus the real molar/volume concentration can be calculated.

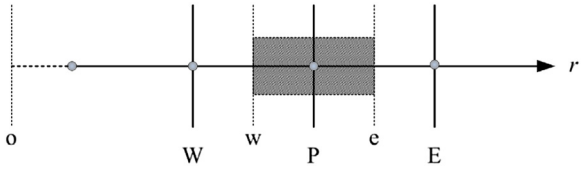

Fig. A1 – Schematic of the discretization of the droplet along its radius.

(1) Mass variation Δm_P (kg) and real concentration ${C_{dP}}^{*}$ of the control volume P

Molar flux of FB gives the mass variation as follows:

$$\Delta m_P \times 10^3 = M_s \cdot \int_t^{t+\Delta t} \left\{ 4\pi D_A r^2 \frac{\partial C_{dP}}{\partial r} |_{we} \right\} \mathrm{d}t \tag{A2}$$

For interior control volumes, Eq. (A2) can be expressed in the discrete form as follows:

$$\Delta m_P = 4\pi \times 10^{-3} M_s \times \left[{D_{Ae}}^0 {r_e}^{02} \frac{{C_{dE}}^{*}(\mathrm{tr}) - {C_{dP}}^{*}(\mathrm{tr})}{\Delta {r_e}^0} - {D_{Aw}}^0 {r_w}^{02} \frac{{C_{dP}}^{*}(\mathrm{tr}) - {C_{dW}}^{*}(\mathrm{tr})}{\Delta {r_w}^0} \right] \Delta t \tag{A2-a}$$

For the control volume at the inner boundary, the discrete form of Eq. (A2) is:

$$\Delta m_P = 4\pi \times 10^{-3} M_s \times \left[{D_{Ae}}^0 {r_e}^{02} \frac{{C_{dE}}^{*}(\mathrm{tr}) - {C_{dP}}^{*}(\mathrm{tr})}{\Delta {r_e}^0} \right] \Delta t \tag{A2-b}$$

And for the control volume at the inner boundary:

$$\Delta m_P = 4\pi \times 10^{-3} M_s \times \left[{R^0}^2 {k_e}^0 \left({C_b}^0 - H^0 {C_{dP}}^{*}(\mathrm{tr}) \right) - {D_{Aw}}^0 {r_w}^{02} \frac{{C_{dP}}^{*}(\mathrm{tr}) - {C_{dW}}^{*}(\mathrm{tr})}{\Delta {r_w}^0} \right] \Delta t \tag{A2-c}$$

The density of the PS/FB solution, ρ_d, had a linear relationship with the mass fraction of FB, w_d, according to experimental results:

$$\rho_d = 1077.01 - 88.5 w_d \tag{A3}$$

With the calculated Δm_P from Eq. (A2) and the function given by Eq. (A3), ${C_{dP}}^{*}$ can be calculated as follows:

$$w_{dP}{}^{*} = \frac{{m_P}^0 + \Delta m_P}{{M_P}^0 + \Delta m_P} \tag{A4}$$

$$\rho_{dP}{}^{*} = 1077.01 - 88.5 w_{dP}{}^{*} \tag{A5}$$

$${C_{dP}}^1 = {\rho_{dP}}^1 \cdot {w_{dP}}^1 \cdot 10^3 / M_s \tag{A6}$$

where M denotes the total mass of the solution, while m denotes the mass of the solvent FB in a control volume.

(2) The volume variation of the control volume

The volume of control volume P at time $t+\Delta t$ was calculated from Δm_P and $\rho_{dP}{}^{*}$ as follows:

$$v_P{}^{*} = \frac{4}{3}\pi \left({r_e}^{*3} - {r_w}^{*3} \right) = \frac{{M_P}^0 + \Delta m_P}{\rho_{dP}{}^{*}} \tag{A7}$$

which gives the length step at time $t+\Delta t$:

$$\Delta r_{P*} = r_e{}^{*} - r_w{}^{*} \tag{A8}$$

The size of the droplet at time $t+\Delta t$ can thus be obtained from $\Delta r_P{}^{*}$.

References

Bile, J., Bolzinger, M.A., Vigne, C., et al., 2015. The parameters influencing the morphology of poly(ε-caprolactone) microspheres and the resulting release of encapsulated drugs. Int. J. Pharm. 494, 152–166.

Bryden, M.D., Brenner, H., 1999. Mass-transfer enhancement via chaotic laminar flow within a droplet. J. Fluid Mech. 379, 319–331.

Chen, C., Norimatsu, T., Takagi, M., Katayama, H., Yamanaka, T., Nakai, S., 1991. Development of foam shells for cryogenic laser fusion target. J. Vac. Sci. Technol. A 9, 340–344.

Freitas, S., Merkle, H.P., Gander, B., 2005. Microencapsulation by solvent extraction/evaporation: reviewing the state of the art of microsphere preparation process technology. J. Control. Release 102, 313–332.

Gharsallaoui, A., Roudaut, G., Chambin, O., et al., 2007. Applications of spray-drying in microencapsulation of food ingredients: an overiew. Food Res. Int. 40, 1107–1121.

Izumikawa, S., Yoshioka, S., Aso, Y., Takeda, Y., 1991. Preparation of poly(L-lactide) microspheres of different crystalline morphology and effect of crystalline morphology on drug release rate. J. Control. Release 15, 133–140.

Jeyanthi, R., Thanoo, B.C., Metha, R.C., DeLuca, P.P., 1996. Effect of solvent removal technique on the matrix characteristics of polylactide/glycolide microspheres for peptide delivery. J. Control. Release 38, 235–244.

Jyothi, N.V.N., Prasanna, P.M., Sakarkar, S.N., et al., 2010. Microencapsulation techniques, factors influencing encapsulation efficiency. J. Microencapsul. 27, 187–197.

Katou, H., Wandrey, A.J., Gander, B., 2008. Kinetics of solvent extraction/evaporation process for PLGA microparticle fabrication. Int. J. Pharm. 364, 45–53.

Kiss, N., Brenn, G., Suzzi, D., Scheler, S., Jennewein, H., Wieser, J., Khinast, J., 2013. The influence of process parameters on the properties of PLGA-microparticles produced by the emulsion extraction method. AIChE J. 59, 1868–1881.

Lai, M.K., Tsiang, R.C., 2004. Encapsulating acetaminophen into poly(L-lactide) microcapsules by solvent-evaporation technique in an O/W emulsion. J. Microencapsul. 21, 307–316.

Lambert, S.M., Overturf, G.E., Wilemski, G., Letts, S.A., Schroen-Carey, D., Cook, R.C., 1997. Fabrication of low-density foam shells from resorcinol-formaldehyde aerogel. J. Appl. Polym. Sci. 65, 2111–2122.

Letts, S.A., Fearon, E.M., Buckley, S.R., Saculla, M.D., Allision, L.M., Cook, R.C., 1995. Preparation of hollow shell ICF targets using a depolymerizing mandrel. Mater. Res. Soc. Symp. Proc. 372, 125–130.

Li, W.I., Anderson, K.W., DeLuca, P.P., 1995a. Kinetic and thermodynamic modeling of the formation of polymeric microspheres using solvent extraction/evaporation method. J. Control. Release 37, 187–198.

Li, W.I., Anderson, K.W., Mehta, R.C., DeLuca, P.P., 1995b. Prediction of solvent removal profile and effect on properties for peptide-loaded PLGA microspheres prepared by solvent extraction/evaporation method. J. Control. Release 37, 199–214.

Li, M., Rouaud, O., Poncelet, D., 2008. Microencapsulation by solvent evaporation: state of the art for process engineering approaches. Int. J. Pharm. 363, 26–39.

Mao, S., Shi, Y., Li, L., Xu, J., Schaper, A., Kissel, T., 2008. Effects of process and formulation parameters on characteristics and internal morphology of poly(D,L-lactide-co-glycolide) microspheres formed by the solvent evaporation method. Eur. J. Pharm. Biopharm. 68, 214–223.

McQuillan, B.W., Nikroo, A., Steinman, D.A., 1997. The PAMS/GDP process for production of ICF target mandrel. Fusion Technol. 31, 381–384.

Michra, K.K., Khardekar, R.K., Singh, R., Pant, H.C., 2002. Fabrication of polystyrene hollow microspheres as laser fusion targets by optimized density-matched emulsion technique and characterization. Pramana: J. Phys. 59, 113–131.

Nazzaro, F., Orlando, P., Fratianni, F., Coppola, R., 2012. Microencapsulation in food science and biotechnology. Curr. Opin. Biotechnol. 23, 182–186.

Paguio, R.R., Nikroo, A., Takagi, M., Acenas, O., 2006. Fabrication and overcoating of divinylbenzene foam shells using dual initiators. J. Appl. Polym. Sci. 101, 2523–2529.

Reuvers, A.J., Smolders, C.A., 1987. Formation of membranes by means of immersion precipitation. 2. The mechanism of formation of membranes prepared from the system cellulose-acetate acetone water. J. Membr. Sci. 34, 67–86.

Shao, T., Feng, X., Wang, W., Jin, Y., Cheng, Y., 2012. Visualization of coupled mass transfer and reaction between gas and a droplet using a novel reactive-PLIF technique. Chem. Eng. J. 200–202, 549–558.

Subramanian, P., Zebib, A., McQuillan, B., 2005. Axisymmetric marangoni convection in microencapsulation. Acta Astronaut. 57, 97–103.

Vasiliauskas, R., Liu, D., Cito, S., 2015. Simple microfluidic approach to fabricate monodisperse hollow microparticles for multidrug delivery. Appl. Mater. Interfaces 7, 14822–14832.

Vay, K., Friess, W., Stefan, S., 2012. A detailed view of microparticle formation by in-process monitoring of the glass transition temperature. Eur. J. Pharm. Biopharm. 81, 399–408.

Vermillion, B.A., Besenbruch, G.E., Brown, L.C., et al., 2004. Microencapsulation studies for mass production of IFE targets. In: General Atomics Report GA-A24431.

Wang, J., 2012. Microfluidic-based synthesis of hydrogel particles for cell microencapsulation and cell-based drug delivery. Polymer 4, 1084–1108.

Yang, Y.Y., Chung, T.S., Ng, N.P., 2001. Morphology, drug distribution, and in vitro release profiles of biodegradable polymeric microspheres containing protein fabricated by double-emulsion solvent extraction/evaporation method. Biomaterials 22, 231–241.